CONCRETE LIBRARY OF JSCE NO. 23, JUNE 1994

TORSIONAL PROPERTIES OF LONG CAISSONS WITH UPPER OPENINGS
(English Translation of Paper in Proceedings of the JSCE, No.466, V-19, 1993)

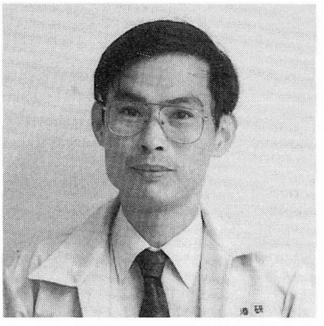

Osamu KIYOMIYA Masao YAMADA

SYNOPSIS

This paper presents test data on the torsional properties of long breakwater caisson models. The specimens were constructed from steel-concrete hybrid components and prestressed concrete components. Since the specimens had upper openings, their torsional characteristics were calculated by mixed torsion analysis taking account of St.Venant torsion and warping torsion. Calculated values were compared with measurements obtained during static torsional loading tests of the specimens. This demonstrated that mixed torsion analysis could accurately evaluate the torsional characteristics of these specimens.

Keywords: torsion, long caisson, hybrid member, pc structure, loading test

---

O.Kiyomiya is the chief of the Structural Mechanics Laboratory at the Port and Harbour Research Institute, Ministry of Transport, Japan. He received his Doctor of Engineering Degree from Tokyo Institute of Technology in 1984. His research interests include structural mechanics in port and harbour constructions. He was awarded a JCI prize in 1991 for a study of the structural design on steel-concrete composite structures. He is a member of JSCE, JCI, and JSSFME.

M.Yamada is a member of the Structural Mechanics Laboratory at the Port and Harbour Research Institute, Ministry of Transport, Japan. He received his Master of Engineering Degree from the University of Tokyo in 1990. His field of research is concrete structural engineering. He is a member of JSCE and JCI.

---

1. INTRODUCTION

The size of marine structures in Japan has been increasing recently. The concrete caissons used for submerged tunnels or breakwaters are now as long as 100m. Such caissons can be fabricated in dry docks or shipyards. and the large-scale construction work involved in placing these caissons at the site has been simplified by the development of large equipment.

If a large-scale caisson is made of reinforced concrete (RC), it becomes too heavy to work with. It is necessary to use structural members of greater strength and ductility than RC to reduce the overall weight. Steel-concrete composite structural members (hybrid members) or prestressed concrete structural members (pc members) are used for that purpose. Figure 1 gives an outline of a long caisson breakwater.

There are certain issues which require investigation from a technical point of view. The torsional properties of a caisson is one such subject, because long caissons are subjected to relatively large torsional moments due to wave forces during towing and unequal subsidence after installation. In the past few marine structures were subjected to substantial torsional moments because the type and size of each structural member was designed to ensure that excessive torsion did not occur. Now, however, torsion has become a problem with today's larger structures.

Some studies have been carried out on the torsion of small concrete beams and large steel structures with closed sections such as the super-structure of bridges or ships. However, the torsional properties of concrete caissons with open cross sections has been studied by only a few researchers.

In this investigation, the load bearing capacity of long caissons subjected to torsion was treated theoretically and experimentally. The torsional properties of long caisson models constructed of hybrid members and pc members were analysed considering St.Venant torsion (circulatory torsion) and warping torsion, and torsional loading tests of these specimens were carried out at the same time. Analytical results were compared with the test results to verify the validity of the analysis method.

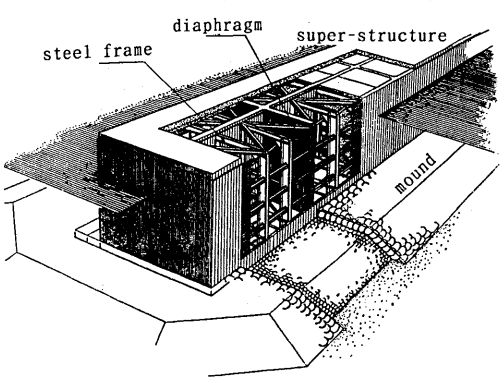

Fig.1 Long caisson breakwater

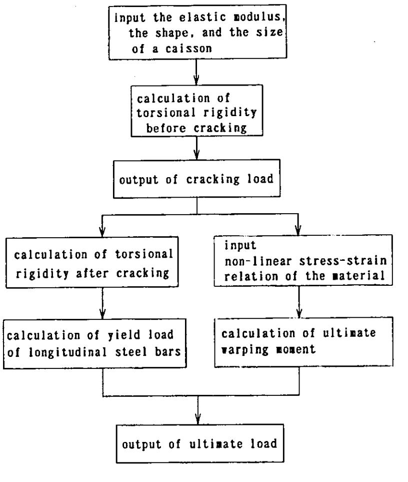

Fig.2 Flow chart for the analysis

2. ANALYSIS

2.1 Governing Equations and Boundary Conditions

Figure 2 is the flow chart of our analysis. The method is based on mixed torsion analysis[1]. Both St.Venant torsion and warping torsion are considered in this mixed torsion analysis.

Warping torsion is usually ignored in the design of concrete structures. The word "warping" can be misunderstood as out-of-plane displacement, but warping torsion actually means the internal torsional moment resulting from shear stress in equilibrium with axial stress arising due to restraint of axial displacement.

When an external torsional moment is applied around the torsional center of a bar member with an upper opening, as shown in Figure 3, the two side walls twist around their own torsional centers as a result of St.Venant torsion and at the same time the vertical displacement at both ends applies a shear force to the walls as in a beam under shear loading. The opposing shear forces in the two walls cause the torsional moment. That is the warping torsional moment.

The direction of the x axis in our analysis is coincident with the longitudinal axis of the member with an upper opening, while the origin of the y and z axes is coincident with the center of gravity of the cross section. The length of the member is l, and does not include the length of the end walls and diaphragms.

When a torsional moment is applied to both ends of the member, the internal torsional moment, T , does not vary along the x axis. This is shown by Eq.1.

$$\frac{dT}{dx}=0 \quad \cdots\cdots (1)$$

Torsion theory for a bar member[2] assumes that the shape of the cross section does not change and that a plane remains a plane as regards displacement in the x direction. The relationship between torsional moment, T , and rotation, ϕ , at a position, x , is represented as Eq.2.

$$T=GJ\frac{d\phi}{dx}-EI_{\omega\omega}\frac{d^3\phi}{dx^3} \quad \cdots\cdots (2)$$

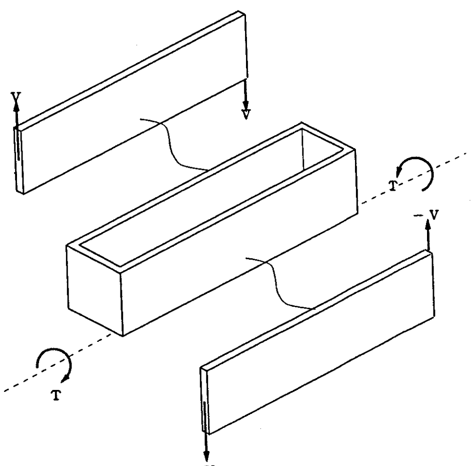

Fig.3 Warping torsion

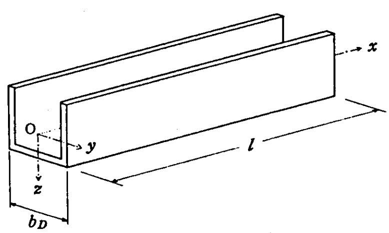

Fig.4 Coordinates for the channel beam

Here, G is shear elastic modulus, J is the St.Venant torsional constant, E is longitudinal elastic modulus, and $I_{\omega\omega}$ is the sectorial moment of inertia. The method of deciding values for J and $I_{\omega\omega}$ is explained later. Equations 1 and 2 lead to the following equation. The common solution of Eq.3 is represented as Eq.4.

$$GJ\frac{d^2\phi}{dx^2}-EI_{\omega\omega}\frac{d^4\phi}{dx^4}=0 \quad (3) \qquad \phi=C_1+C_2\frac{x}{l}+C_3\cosh ax+C_4\sinh ax \quad (4)$$

Boundary conditions for the rotation at the both ends are represented by Eq.5 and Eq.6, here $\bar{\phi}$ is the rotation applied at both ends.

$$\phi=\bar{\phi} \qquad (x=0) \quad (5)$$

$$\phi=-\bar{\phi} \qquad (x=l) \quad (6)$$

Warping of the cross section is restrained by the end walls in an actual structure. The effect of this restraint is represented by following equations according to Hsu's method[3].

$$EI_{\omega\omega}\frac{d^2\phi}{dx^2}=GJ_Db_D\frac{d\phi}{dx} \qquad (x=0) \quad (7)$$

$$-EI_{\omega\omega}\frac{d^2\phi}{dx^2}=GJ_Db_D\frac{d\phi}{dx} \qquad (x=l) \quad (8)$$

where, J_D is the St.Venant torsional rigidity of an end wall around the y axis, and b_D is the length of the end wall in the y direction.

The values of C_1, C_2, C_3, and C_4 are set by the boundary conditions Eq.5. Eq.6, Eq.7. and Eq.8. Thus the relationship between T and ϕ at each position x is obtained.

2.2 Torsional Rigidity before Cracking

a) St.Venant torsional rigidity

When a bar member with a thin rectangular cross section is subjected to torsion. the distribution of shear strain, ε_{zx}, is represented by Eq.9 and the distribution of shear stress, σ_{zx}, is represented by Eq.10.

$$\varepsilon_{zx}=y\frac{d\phi}{dx} \quad (9)$$

$$\sigma_{zx}=2G\varepsilon_{zx}=2Gy\frac{d\phi}{dx} \quad (10)$$

The St.Venant torsional moment, T_s, is obtained by integrating this shear stress along the y axis,

$$T_s=GJ\frac{d\phi}{dx} \quad (11)$$

where St.Venant torsional constant, J . is given by the following equation:

$$J=\frac{1}{3}bt^3 \quad (12)$$

where b is the breadth and t is the thickness of the cross section.

St.Venant torsional rigidity of a hybrid member has never been calculated. Thus it was assumed using the following simple method in this report.
Let t be the thickness of a hybrid member and $t_c(=r_ct)$ be the thickness of concrete and $t_s(=r_st)$ the thickness of steel plate, where $r_c+r_s=1$. G_c is the

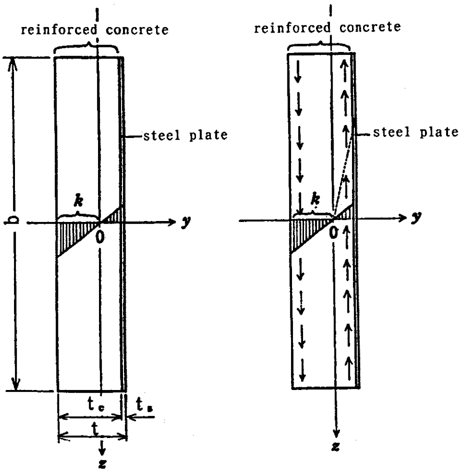

a) shear strain b) shear stress

Fig.5 Distributions of strain and stress

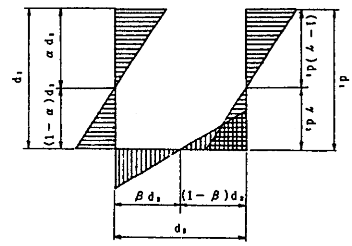

Fig.6 Distribution of ω for a uniform channel section

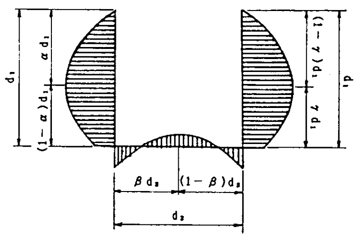

Fig.7 Distribution of warping shear flow

shear elastic modulus of the concrete, G_s is the shear elastic modulus of the steel plate, and g is the ratio of the two shear elastic moduli , $g=G_s/G_c$.

The distribution of shear strain due to torsion is assumed to be linear, as shown in Fig.5(a). The y coordinate is normal to the plate, and y equals to 0 at the neutral axis and $-k$ at the concrete surface. Thus, the distribution of shear stress is as shown in Fig.5(b) and is given by the following equation:

$$\sigma_{zx}=2G_c y\frac{d\phi}{dx} \qquad (y\leqq t_c-k)$$

$$=2G_s y\frac{d\phi}{dx} \qquad (y>t_c-k) \cdots\cdots\cdots\cdots (13)$$

Equation 14 is derived from the condition that the total shear force equals zero.

$$\int_{-k}^{t-k}\sigma_{zx}b\,dy=0 \cdots\cdots\cdots\cdots (14)$$

The following equation is obtained by integrating Eq.14.

$$k=\frac{(2gr_s r_c+gr_s^2+r_c^2)}{2(gr_s+r_c)}t \cdots\cdots\cdots\cdots (15)$$

The torsional moment is obtained by integrating the shear stress with respect to y axis. Thus, the St.Venant torsional rigidity of a hybrid member, $(GJ)_{com}$, can be represented by Eq.16.

$$(GJ)_{com}=G_c\cdot\frac{4}{3}b[\{(r_c t-k)^3+k^3\}+g\{(t-k)^3-(r_c t-k)^3\}] \cdots\cdots\cdots\cdots (16)$$

Although the validity of this equation needs to be verified by torsional loading tests of a plate member, this verification has not yet carried out.

b) Warping torsional rigidity

Warping torsional rigidity is the product of longitudinal elastic modulus, E, and sectorial moment of inertia, $I_{\omega\omega}$. $I_{\omega\omega}$ is defined as Eq.17 and is a function of the form and the dimensions of the cross section.

$$I_{\omega\omega} \equiv \int_A \omega^2 dA \cdots\cdots(17)$$

ω is called the sectorial area coordinate and it represents displacement in the x direction when the angle of rotation over a unit length equals unity. The distribution of ω in a cross section with an upper opening can be calculated under the condition that the axial force $\Sigma F=0$, the bending moment around y axis $\Sigma My=0$, and the bending moment around the z axis $\Sigma Mz=0$. When the member is made of a uniform material and the thickness is constant, the neutral axis ratios at three plates, α, β, and γ, are 0.568, 0.5, and 0.432, respectively.

For a hybrid member, $I_{\omega\omega}$ is obtained from the cross-sectional area considering the ratio of longitudinal elastic modulus of steel plate to concrete.

From the definition of ω, longitudinal stress, σ_{xx}, is represented as Eq.18. Cracks due to this stress are called warping bending cracks in this report.

$$\sigma_{xx} = -E\omega \frac{d^2\phi}{dx^2} \cdots\cdots(18)$$

The value of shear flow which forms the warping torsional moment is obtained from Eq.19.

$$\sigma_{sx} t = EQ_\omega \frac{d^3\phi}{dx^3} \cdots\cdots(19)$$

Here Q_ω is obtained from the integration of ω as represented in Eq.20 along the s coordinate--which coincides with the center line of the plates--and is called the sectorial static moment of the cut-off portion.

$$Q_\omega = \int_{s_e}^{s} \omega dA \cdots\cdots(20)$$

Here s_e is the starting point of the integration and is placed at the end of the cross section where the shear stress is usually zero. The distribution of Q_ω in a cross section with an upper opening is as shown in Fig.7, and Q_ω peaks at the neutral axis of ω.

The shear stress in a cross section with an upper opening is obtained as the sum of the shear stresses due to St.Venant torsion and warping torsion. Cracking occurs when the value of shear stress reaches the tensile strength of the concrete. Such cracking is called torsional shear cracking in this report in order to make clear the difference between it and the warping bending cracks mentioned above. The load at which a crack occurs in a pc member is calculated considering the compressive stress on the concrete.

2.3 Torsional Rigidity after Cracking

a) St.Venant torsional rigidity

A space truss model is usually used to calculate the St.Venant torsional rigidity of a RC member after cracking. In this model, the concrete between cracks is considered as a diagonal compression member and the steel bars are considered tension members in a truss. Collins et al[1] used an equation in which St.Venant rigidity is obtained from the ratio of reinforcement in the longitudinal and lateral directions, the elastic modulus of the reinforcement, and the perimeter of the shear flow path. This method is applied to the calculation of the St.Venant torsional rigidity of pc members.

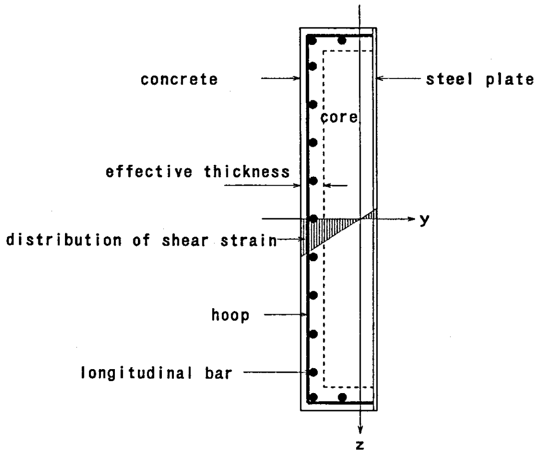

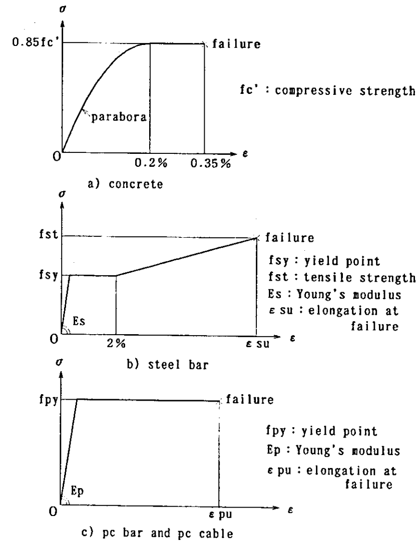

On the other hand, the distribution of shear strain due to St.Venant torsion after cracking for a hybrid member is assumed as in Fig.8. The core of the cross section is assumed to have no effect on torsional strength. The effective thickness for torsional strength is assumed to be $0.75A_0/P_0$ according to the method used by Collins et al[1] for RC members. Here, A_0 is the area enclosed by the shear flow, and P_0 is the perimeter of the shear flow path. The shear flow path is assumed to coincide with the center line of the hoops and the steel plate.

The shear rigidity of the effective thickness is calculated using the same method as for the shear rigidity of a cracked RC plate. The position of the neutral axis of shear strain is calculated from the ratio of the shear rigidity of effective thickness and the steel plate as before cracking. The St.Venant torsional rigidity is calculated based on this distribution of shear strain.

b) Warping torsional rigidity

The distribution of sectorial area coordinates ω changes after cracking. The method of calculating the distribution of ω after cracking is described in detail in the appendix of the paper by Hsu et al[3]. The neutral axis ratios α, β, and γ in the three walls are assumed, and the axial force, ΣF, the bending moment around the y axis, Σ My, and the bending moment around the z axis, Σ Mz are calculated. Values of α, β, and γ are varied until the conditions ΣF=0, ΣMy=0, ΣMz=0 are satisfied. Hsu et al[3] called this method the bi-material model; the concrete in the tensile region is neglected and the area of steel is replaced by the equivalent area of concrete according to the ratio of elastic modulus. Warping torsional rigidity is calculated using this bi-material model, since the plasticity of the concrete can be neglected up to the steel yield point.

c) Yielding of steel

The load at which the longitudinal steel starts to yield can be calculated as the load at which the maximum strain due to warping reaches the yield strain.

The load at which the hoops start to yield due to shear strain can be calculated as follows. The shear strain due to St.Venant torsion is represented by Eq.21.

$$\varepsilon_{zx,CR,S}=k_{CR}\frac{d\phi}{dx}\cdots\cdots(21)$$

Here, k_{CR} is the distance between the reinforcement and the neutral axis of shear strain after cracking. The shear strain due to warping torsion is represented by Eq.22,

$$\varepsilon_{zx,CR,\omega}=\frac{EQ_\omega}{G_st_s+G_{CR}t_{CR}}\frac{d^3\phi}{dx^3}\cdots\cdots(22)$$

where G_{CR} is the shear rigidity of the effective thickness described in (3)a), and t_{CR} is the effective thickness. The total shear strain, which is the sum of Eq.21 and Eq.22, has a maximum at $x=l/2$.

2.4 Ultimate Load

Since many reinforcing bars are distributed in the side walls and bottom plate, failure does not occur when a single reinforcing bar starts to yield. The ultimate load is calculated as the load at which the strain of the concrete in compression reaches the ultimate compressive strain. The distribution of ω is calculated at compressive failure of the joint between the cross section and the end wall where $x=0$. The position of the neutral axis of ω is found using the condition $\Sigma F=0$, $\Sigma My=0$, and $\Sigma Mz=0$ as described above. Nonlinearity is taken into consideration in the relationship between stress and strain of the concrete and steel. The stress-strain relationship shown in Fig.9 is used in this calculation.

The ultimate value of $I_{\omega\omega}$ is calculated from Eq.17 using the resulting distribution of ω. The area of each small element is calculated using its secant elastic modulus for area integration. The value of the second derivative of angle of rotation is calculated as the strain divided by the sectorial area coordinate.

$$\frac{d^2\phi}{dx^2}=\varepsilon/\omega\cdots\cdots(23)$$

The ultimate warping moment is calculated from Eq.24.

$$M_\omega=EI_{\omega\omega}\frac{d^2\phi}{dx^2}\cdots\cdots(24)$$

The relationship between warping moment and warping torsional moment is shown by Eq.25.

$$T_\omega=2M_\omega/l\cdots\cdots(25)$$

Since the ultimate St.Venant torsional moment at the end is very small and the external torsional moment is resisted almost only by the warping torsional moment, the ultimate torsional moment is determined by the ultimate warping torsional moment calculated using Eq.25.

The ultimate loads as calculated from the ultimate warping moment and from the load at which the hoops yield are compared, and the lower value is taken as the ultimate load for the specimen.

3. LOADING TESTS

3.1 Structure of the Specimens[4]-[6]

Two specimens of hybrid caissons and four specimens of pc caissons were used for the tests. The basic dimensions of the specimens were 5.3m long, 1.0m high, and 1.0m wide. They are shown in Fig.10. The cross section was open at the top, and the thickness of the side walls and the bottom plates was 10cm. The end walls were 350mm thick.

Open-sandwich composite panels were used for the side walls, the bottom plates, and the end walls of the hybrid caisson specimens. In these panels, the steel plate and RC are connected mechanically by shear connectors. Ribbed steel plates 6mm in thickness were used as diaphragms. One diaphragm was used for specimen No.1 and three diaphragms for specimen No.2.

Figure 11 is a side view of the reinforcing bar arrangement for a hybrid caisson specimen. As shear connectors, angle ribs of size 40mm and thickness 3mm and J shape deformed bars of diameter 6mm were welded on at 150mm centers. The concrete reinforcement was deformed bars of diameter 6mm at a spacing of 75mm in both longitudinal and lateral directions. The cover over the reinforcing bars was 20mm.

In the case of specimen No.3, the walls were pc plates and the diaphragms were fabricated with H-shaped steel. Figure 12 shows the bar arrangement for the open cross section of this specimen. Deformed bars of diameter 6mm were arranged in pairs at a spacing of 150mm in the longitudinal direction. In the lateral direction, deformed bars of the same diameter were arranged in pairs at a spacing of 75mm. Sixteen pc cables were included and given a tensile stress of 111.5kgf/mm². Thus, a prestress of about 30kgf/cm² was applied to the concrete.

Table 1 Test Specimens

Specimen	side wall	diaphragm	joint
No. 1	composite panel	1 steel plate	no joint
No. 2	composite panel	3 steel plates	no joint
No. 3	prestressed concrete	H-shape steel	no joint
No. 4	prestressed concrete	reinforced concrete	no joint
No. 5	prestressed concrete	reinforced concrete	match cast joint
No. 6	prestressed concrete	reinforced concrete	filled with mortar

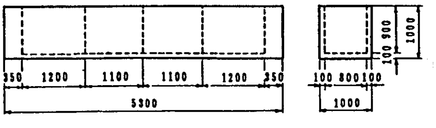

Fig.10 Dimensions of specimen No.2

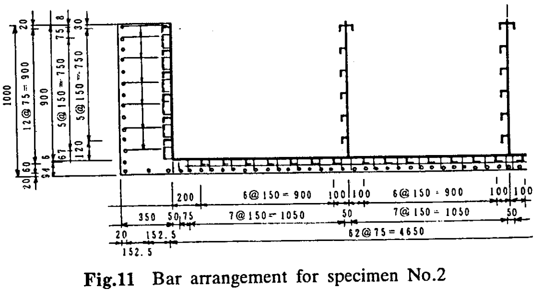

Fig.11 Bar arrangement for specimen No.2

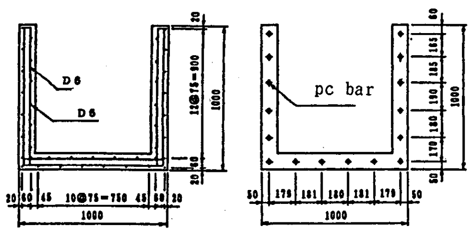

Fig.12 Bar arrangement for specimen No.3

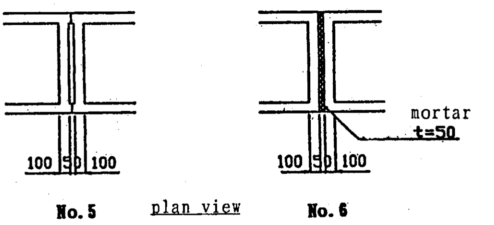

Fig.13 Joints for specimen No.5 and No.6

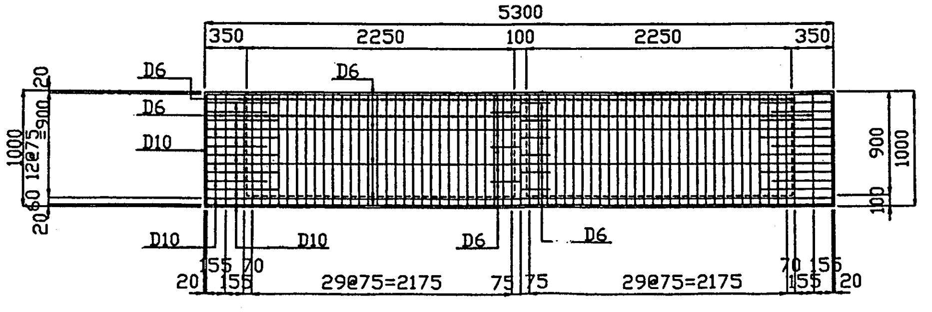

Fig.14 Bar arrangement for specimen No.4

For specimens No.4-6, the walls were pc plates and diaphragms were RC plates. Specimen No.4 had no joints, while No.5 had a match cast joint and No.6 had a joint filled with mortar. Figure 13 gives details of these joints. Figure 14 shows the bar arrangement for the side walls of these specimens. Deformed bars of diameter 6mm were arranged in pairs at a spacing of 300mm in the longitudinal direction. In the lateral direction, deformed bars of the same diameter were arranged in pairs at a spacing of 75mm. Ten pc bars were incorporated in specimen No.4 and thirteen in the No.5 and No.6 specimens, and these pc bars were given a tensile stress of $64.0kgf/mm^2$. Thus, a prestress of about $15kgf/cm^2$ was applied to the concrete of No.4 specimen and about $20kgf/cm^2$ to the concrete of No.5 and No.6.

Deformed bars of diameter 10mm were arranged at a spacing of 75mm in the longitudinal direction in addition to the 6mm bars near the joints of the end walls and the open cross section.

3.2 Mechanical Properties of the Material

Table 2 shows the results of tensile tests carried out on the steel used for the specimens.

The concrete base slump was 15cm and the maximum aggregate size was 10mm. Table 3 gives the compressive strength of the concrete.

3.3 Loading Test Procedure

Figure 15 and Photo 1 show the loading arrangement. Rotation was applied to both ends of the specimens statically using two hydraulic jacks. Universal joints formed the support points. At one support, the specimen was free to move in the longitudinal direction. The connections between the jacks and

Table 2 Tensile Test Results of the Steel

steel	yield point (kgf/mm²)	tensile strength (kgf/mm²)	elongation at failure (%)	Young's modulus (kgf/mm²)
deformed bar (6mm)	37.8	51.4	25.6	2.03×10^4
deformed bar(10mm)	32.9	48.2	28.9	2.02×10^4
steel plate (6mm)	34.3	44.9	39.9	2.14×10^4
L-shape rib	37.2	49.9	29.8	2.14×10^4
pc bar	114.3	116.7	13.0	2.03×10^4
pc cable	184.1	201.5	7.1	2.00×10^4

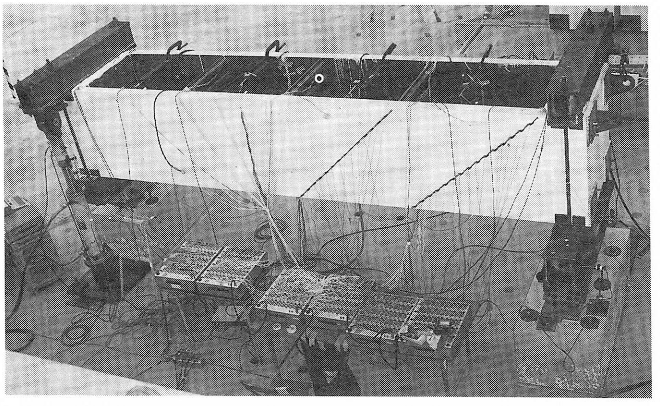

Photo 1 Specimen No.2 during test

Table 3 Compressive Strength of the Concrete

specimen	compressive strength (kgf/cm²)
No. 1	284
No. 2	308
No. 3	355
No. 4	479
No. 5	460
No. 6	394

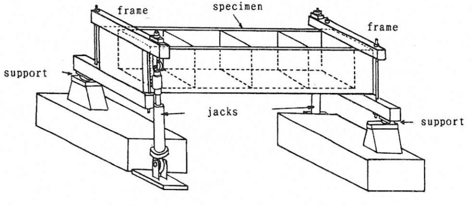

Fig.15 Loading set-up

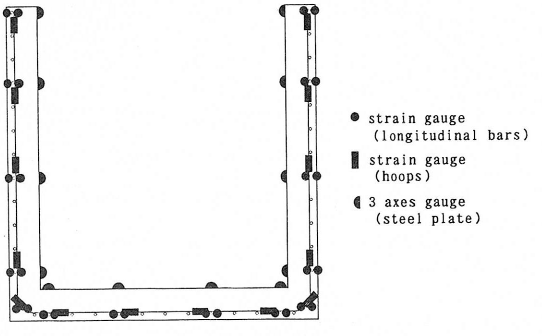

Fig.16 Arrangement of strain gauges

steel frames were universal joints to ensure that no external forces aside from the torsional moment was applied.

3.4 Measurement Procedure

The applied load was measured using load cells installed on the jacks. Changes in the length of the jack axis were measured with displacement transducers. Torsional rotation around the longitudinal axis of the specimens was measured with inclinometers: the sensitivity of these instruments was 200 microstrain per degree so that small rotations could be measured. Strain on the steel was measured using strain gauges mounted at the center cross sections between diaphragms. Figure 16 shows the position of strain measurements in the case of the hybrid specimens. Almost the same number of gauges was used for the other specimens.

4. RESULTS OF LOADING TESTS

Figure 17 shows the relationship between applied load and rotation at the specimen ends. The relationship between applied load and torsional moment is given by Eq.26.

$$T = P \cdot l_a + T_d \cdots\cdots (26)$$

where T: torsional moment; P: load ; l_a: distance between the jack and support; T_d: torsional moment due to the weight of the specimen itself; W: weight of the specimen. $T_d = W \cdot l_a / 4$

The rotation shown in Fig.17 was calculated from the measured changes in the length of the jack axis, and this rotation was almost the same as that measured by inclinometers at the end of the specimens.

The first crack appeared at the corner where the open cross section and the end wall met, then cracks were observed on the exterior of the side walls. Cracks were also observed at the corners of the RC diaphragms. Diagonal cracks were seen on side walls, bottom plates, end walls, and RC diaphragms. The number of cracks increased as the load increased.

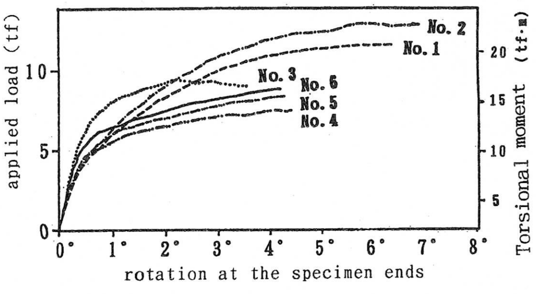

Fig.17 Relationship between load and rotation

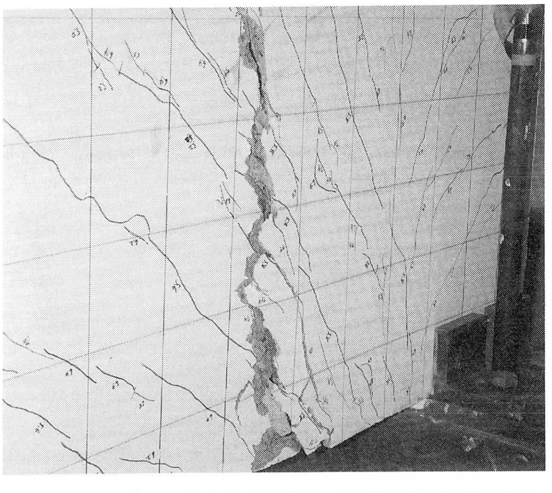

Photo 2 Failure of specimen No.4

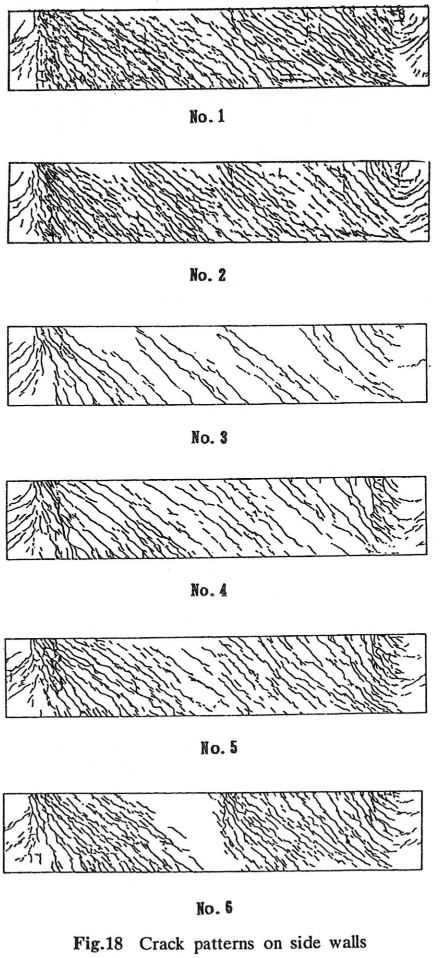

Fig.18 Crack patterns on side walls

In the case of specimens No.1 and No.2, the concrete struts between cracks on the side walls failed after the strain on the hoops in the side walls reached the yield strain. On the other hand, in the case of pc specimens Nos.3 to 6, the concrete forming the side walls near the end wall failed (see photo 2) after the longitudinal reinforcing bars near the end wall yielded.

In the case of hybrid specimens, the ribs welded to the diaphragms buckled when the load was still small. The steel plate and the concrete in the end wall separated in the ultimate state. The shear connectors were found not to have failed when observed after the loading test. The ultimate load on No.2 specimen, which had three diaphragms, was more than that on No.1, with the difference being about 10%.

Diagonal shear cracks occurred when the rotation at the end reached about 0.3 degrees, and then the torsional rigidity decreased. The minimum ultimate rotation at the end was 3.57 degrees--in the case of specimen No.3--while the maximum value was 6.89 degrees for No.2. Since the span was 5.0m, the ultimate average angle of rotation per unit length was as much as 1.43 degrees per meter for No.3 and 2.76 degrees per meter for No.2. Thus a long caisson was found to have considerable ductility.

Figure 18 shows a side view of the crack pattern at the ultimate state. The angle of the cracks is about 45 degrees to the longitudinal axis. On the end walls, the cracks are perpendicular to those on the side walls.

The number of cracks in hybrid specimens Nos.1 and 2 was greater than that in the pc specimens Nos.3 to 6. The density of cracks in hybrid specimens was also greater than that in pc specimens when compared at the same angle of rotation.

The crack patterns of Nos.5 and 6 show that separation was not observed at the joints. The load bearing capacity of the joints used in these specimens was thus satisfactory.

5.DISCUSSIONS

Table 4 shows the test results and the calculation results for cracking load and ultimate load.

Table 4 Test Results and Calculation Results

specimen	Cracking Load(tf)				Ultimate Load (tf)	
	Test		Calculation		Test	Calculation
	warping	torsion	warping	torsion		
No. 1	1.04	2.02	0.97	2.11	11.70	11.73
No. 2	1.21	2.59	0.75	2.68	13.10	11.91
No. 3	4.94	5.93	4.35	5.02	9.46	9.10
No. 4	3.25	3.45	3.17	3.74	7.46	7.28
No. 5	3.95	3.17	3.38	4.29	8.43	7.95
No. 6	4.77	3.99	3.06	3.85	8.78	7.79

The crack patterns indicate that cracks on the end walls are perpendicular to those on the side walls. This proves that the end walls are subjected to torsion around the y axis as a result of the restraint on warping of the open cross section. Although the failure modes of the hybrid and pc specimens were similar, certain differences between them were clarified through analysis.

For hybrid specimens, end failure due to the restraint on warping did not happen, since the ratio of steel to concrete was large in the longitudinal direction. Instead, the density of cracks was greater and the hoops yielded, since the neutral axis of shear strain shifted toward the steel plate.

Figure 19 shows the distribution of strain in the hoops and the lateral strain on the internal steel plate of hybrid specimen No.2. The hoop strain was much more than that on the internal steel plate, so the hoops yielded. The strain on the steel plate was generally small.

The neutral axis of shear strain was used to calculate the St. Venant torsional rigidity of hybrid specimens. The neutral axis ratio, defined as the ratio of the distance between the neutral axis and the surface of the concrete to the distance between the neutral axis and the surface of the steel plate, was assumed to be 13.2. A higher value of neutral axis ratio means that the neutral axis is nearer the steel plate. Figure 20 shows the relationship between applied load and the ratio of the strain on the hoops to that on the steel plate. As the load increased, this ratio increased. Thus the neutral axis shifted toward the steel plate. Figure 20 shows that the value of 13.2 as the neutral axis ratio was suitable for calculation of St. Venant torsional rigidity of hybrid specimens.

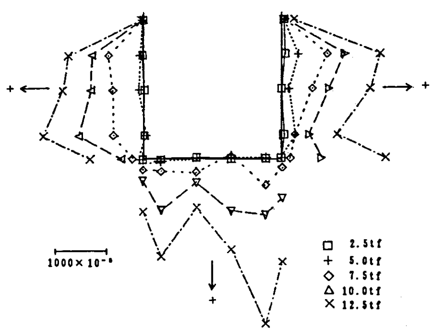

a) strain of a stirrup

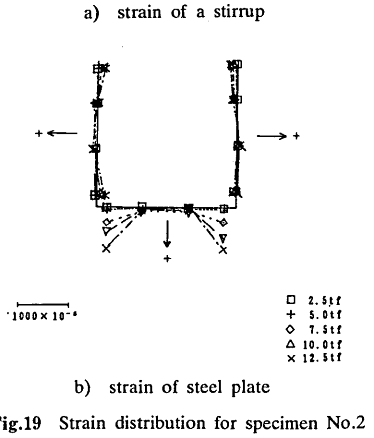

b) strain of steel plate

Fig.19 Strain distribution for specimen No.2

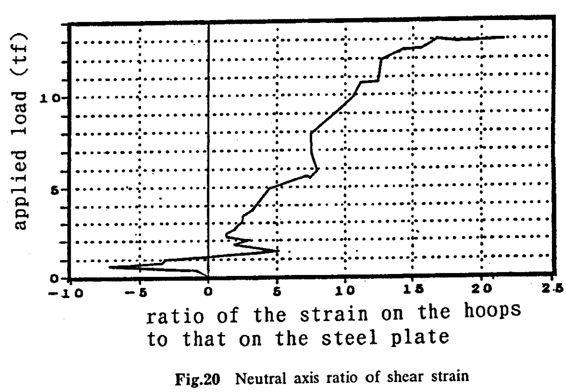

Fig.20 Neutral axis ratio of shear strain

Although some assumptions were made in analyzing the hybrid specimens--that the distribution of shear strain was linear, that the bi-material model could be applied to hybrid members, that the strain due to St.Venant torsion and warping torsion could be simply added to calculate the strain of steel bars, and that the yield load of steel bars equaled the ultimate load--Table 4 shows that this analysis approximately estimated the torsional cracking load and the torsional limit of hybrid specimens.

On the other hand, in pc specimens where the steel ratio was relatively small, the longitudinal steel bars yielded due to the restraint on warping and the concrete in compressive area failed. Table 4 shows that the analysis was able to approximately estimate the torsional cracking load and the torsional limit. The torsional limit was calculated from the ultimate warping moment near the end of the specimen. Thus, reinforcement of the end effectively increases the torsional limit in the case of pc caissons.

6.CONCLUSIONS

The following conclusions were reached in this research:

(1) Cracks occurred at an angle of 45 degrees to the longitudinal axis, and the torsional rigidity fell considerably after cracking. The ultimate angle of rotation at the end was more than 3.5 degrees, giving an ultimate angle of rotation per unit length of more than 1.4 degrees per meter. This demonstrates that caissons with upper openings made with hybrid members and pc members are considerably ductile. The diaphragms did not have a significant effect on the ultimate load and the failure mode.

(2) For hybrid specimens, in which the steel ratio was relatively high, the neutral axis of shear strain shifted toward the steel plate as the load increased and the hoops yielded. Although the analysis--in which St.Venant torsion and warping torsion were considered and steel was replaced with concrete in the ratio of their elastic moduli--included some assumptions, it was able to approximately estimate the cracking load, the ultimate load, and the failure mode for the two specimens.

(3) For pc specimens, in which the steel ratio was relatively law, the concrete failed by compression due to the restraint on warping near the end. A method of calculating the ultimate warping moment by considering the nonlinearity of the materials was able to estimate the ultimate load of four specimens conservatively. It was found that reinforcement of the end effectively increases the torsional limit.

(4) At joints in the pc specimens, no separation was observed. The joints used in these specimens had satisfactory strength.

7. POSTSCRIPT

We hope that this paper will be of some help in the development of more rational calculation methods for the torsional properties of concrete structures with open cross sections.

ACKNOWLEDGEMENT

The test specimens were made by Nippon Kokan K.K. ,Mitsui Zosen K.K., and P.S.Corporation.

REFERENCES

[1] Krpan, P. and Collins, M.P: Predicting Torsional Response of Thin-Walled Open RC Members, Journal of the Structural Division, Proceedings of the ASCE, Vol.107, No.ST6, pp.1107-1127, June 1981

[2] Nishino, F and Hasegawa, A: Elastic Analysis of Structures, JSCE, pp.257-307, 1983 (in Japanese)

[3] Hwang, C.S and Hsu, T.T.C.: Mixed Torsion Analysis of Reinforced Concrete Channel Beams - A Fourier Series Approach, ACI Journal, pp.377-386, Sep.-Oct. 1983

[4] Yamada, M, Kiyomiya, O, and Yokota, H: Torsional Properties of Long Caissons Fabricated by Hybrid Members, Transactions of the JCI, Vol.13, pp.547-552, 1991

[5] Kiyomiya, O, Yamada, M, and Yoshimura, T: Study on the Torsion of Long PC Caissons, Proceedings of JCI Symposium, pp.31-36, July 1991 (in Japanese)

[6] Nakada, K, Kiyomiya, O, and Yamada, M: Torsional Properties of Long PC Caissons with Joints, Proceedings of JSCE Annual Conference No.5, pp.724-725, Sep. 1991 (in Japanese)